

# Quantum spin Hall states in graphene interacting with WS<sub>2</sub> or WSe<sub>2</sub>

T. P. Kaloni<sup>1,\*</sup>, L. Kou<sup>2</sup>, T. Frauenheim<sup>2</sup>, and U. Schwingenschlögl<sup>1,†</sup>

<sup>1</sup>*Physical Science & Engineering Division, KAUST,*

*Thuwal 23955-6900, Kingdom of Saudi Arabia and*

<sup>2</sup>*Bremen Center for computational Materials Science,*

*University of Bremen, Am Falturm 1, 28359, Bremen, Germany*

## Abstract

In the framework of first-principles calculations, we investigate the structural and electronic properties of graphene in contact with as well as sandwiched between WS<sub>2</sub> and WSe<sub>2</sub> monolayers. We report the modification of the band characteristics due to the interaction at the interface and demonstrate that the presence of the dichalcogenides results in quantum spin Hall states in the absence of a magnetic field.

## I. INTRODUCTION

Research on graphene today appears to have reached a peak, mainly because the material is rather difficult to be utilized in electronic devices due to limitations in high quality mass production. Thus, interest is shifting to hybrid systems with other two-dimensional materials, both for application purposes and to create opportunities to better understand basic physical and chemical phenomena<sup>1,2</sup>. Heterostructures of semiconducting MoS<sub>2</sub> and graphene already have been demonstrated, showing potential particularly in data storage<sup>3</sup>. Moreover, the joint two-dimensional nature of the two components can be utilized for fabricating large scale flexible nanoelectronic devices. For example, a new generation of field effect transistors based on heterostructures of WS<sub>2</sub> and graphene on transparent and flexible substrates has shown a promising performance<sup>4</sup>.

Two-dimensional topological insulators in a quantum spin Hall (QSH) state have metallic edges that sustain dissipationless current flow<sup>5,6</sup>. For graphene this effect has been predicted by Kane and Mele using an analytical model<sup>7</sup>. Since the energy gap of graphene is tiny ( $\sim 10^{-3}$  meV) due to the small intrinsic spin-orbit coupling (SOC)<sup>8</sup>, experimental observation of the QSH state is difficult. Various ideas promising an enhancement have been put forward, all based on proximity to areas in that the electrons are subject to strong SOC, including heavy atom deposition<sup>9</sup>, H adsorption<sup>10</sup>, and heterostructures with MoTe<sub>2</sub> and Bi<sub>2</sub>Te<sub>3</sub><sup>11</sup>.

Experimental realization of a QSH state in the topological insulator HgTe<sup>5</sup> has initiated efforts on other materials, in particular on graphene. Recently, experiments have demonstrated that graphene in a strong magnetic field supports also a QSH state, which is interesting for novel quantum circuits<sup>12</sup>. However, the experimental difficulties coming along with large magnetic fields<sup>13</sup> call for alternative approaches. In this work we propose hybrid structures that host a QSH state in the absence of a magnetic field. Specifically, we employ density functional theory (including van der Waals corrections) to study the following systems: (a) graphene on WS<sub>2</sub> or WSe<sub>2</sub> and (b) graphene sandwiched between two WS<sub>2</sub> or WSe<sub>2</sub> layers. Our results prevail that the SOC in graphene can be enhanced such that a reasonable energy gap is achieved at the K/K' points with large band splitting. QSH states are demonstrated for the sandwich systems.

## II. COMPUTATIONAL DETAILS

The heterostructures are constructed by joining a  $4 \times 4 \times 1$  supercell of graphene with  $3 \times 3 \times 1$  supercells of the dichalcogenides. A vacuum layer of at least  $15 \text{ \AA}$  thickness guarantees that there is no artificial interaction perpendicular to the two-dimensional system due to the periodic boundary conditions. For the structural relaxation we employ the Quantum-ESPRESSO code<sup>14</sup>, using the generalized gradient approximation (GGA), in order to include the van der Waals forces. The atomic positions are optimized until all forces have converged to less than  $0.005 \text{ eV/\AA}$ . The electronic structure calculations then are performed using the Vienna Ab-initio Simulation Package<sup>15</sup> both with pure GGA and including the spin. A plane wave cutoff energy of  $450 \text{ eV}$  and a Monkhorst-Pack  $16 \times 16 \times 1$  k-mesh are employed.

## III. RESULTS AND DISCUSSION

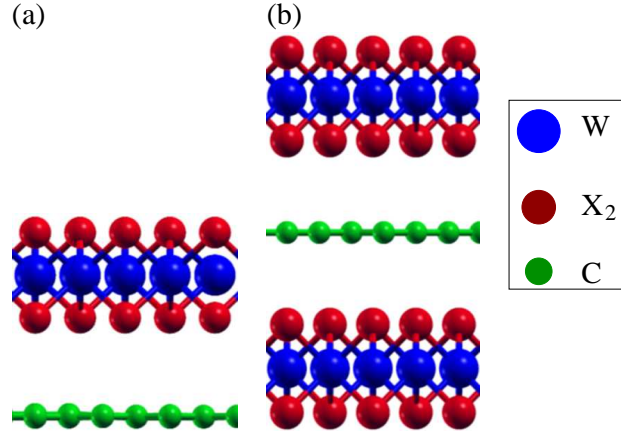


FIG. 1. (a) Graphene in contact with one dichalcogenide monolayer. (b) Graphene sandwiched between two dichalcogenide monolayers.

The systems under consideration are illustrated in Fig. 1. The lattice parameters of the graphene ( $9.98 \text{ \AA}$ ) and  $\text{WS}_2$  supercells ( $9.57 \text{ \AA}$ ) give rise to a lattice mismatch of  $2.7\%$ . The distance between the two subsystems converges to  $d = 3.41 \text{ \AA}$ , see Table I, which is a typical value for graphene on a semiconducting substrate. We observe no modification of the C–C bond lengths, whereas the W–S bond lengths ( $2.45 \text{ \AA}$  to  $2.46 \text{ \AA}$ ) are modified as compared to pristine  $\text{WS}_2$  ( $2.39 \text{ \AA}$ <sup>16</sup>) because of the lattice mismatch. We find  $d = 3.42 \text{ \AA}$  for graphene on  $\text{WSe}_2$  with a C–C bond length of  $1.42 \text{ \AA}$ , which is the value of pristine graphene. The

TABLE 1. Distance between the subsystems ( $d$ ), binding energy per C atom ( $E_b$ ), band gap ( $E_g$ ), valance band splitting ( $\Delta_v$ ), and conduction band splitting ( $\Delta_c$ ).

	GGA			GGA+SOC		
System	$d$ (Å)	$E_b$ (meV)	$E_g$ (meV)	$E_g$ (meV)	$\Delta_v$ (meV)	$\Delta_c$ (meV)
Graphene/WS <sub>2</sub>	3.41	53	0.9	0.7	33	33
WS <sub>2</sub> /Graphene/WS <sub>2</sub>	3.40	51	0.1	1.1	92	99
Graphene/WSe <sub>2</sub>	3.42	54	3.6	0.9	145	132
WSe <sub>2</sub> /Graphene/WSe <sub>2</sub>	3.42	52	3.0	1.0	149	153

W–Se bond length (2.52 Å to 2.53 Å) is almost the same as in pristine WSe<sub>2</sub> (2.52 Å<sup>16</sup>). Moreover, we obtain  $d = 3.40$  Å and  $d = 3.42$  Å for graphene sandwiched between WS<sub>2</sub> and WSe<sub>2</sub> layers, respectively, whereas the other structural parameters are the same as for the simple contacts.

Graphene is zero-gap semiconductor with very weak SOC<sup>17</sup>. On the other hand, WS<sub>2</sub> is semiconductor with a direct band gap of 1.30-1.35 eV<sup>18</sup>. Its structural and electronic properties have been studied extensively, see Ref.<sup>19</sup> and the references therein. WS<sub>2</sub> is widely utilized for  $n/p$ -doped field effect transistors, for example<sup>20</sup>. Experimentally, the synthesis and characterization of graphene on WS<sub>2</sub> has been reported in Ref.<sup>4</sup>. The authors claim that a device based on this system can operate at room temperature with good current modulating capacity. We show in Fig. 2(a) the band structure obtained for graphene on WS<sub>2</sub> without SOC, demonstrating some interaction between the two subsystems, though without chemical bonding. The binding energy

$$E_{\text{binding}} = E_{\text{graphene/WS}_2} - E_{\text{WS}_2} - E_{\text{graphene}},$$

where  $E_{\text{graphene/WS}_2}$ ,  $E_{\text{WS}_2}$ , and  $E_{\text{graphene}}$  are the total energies of the hybrid structure, WS<sub>2</sub>, and graphene, respectively, amounts to 53 meV per C atom, in agreement with Ref.<sup>21</sup>. Due to this weak interaction, a small band gap of 0.9 meV is obtained, see the zoomed view in Fig. 2(a), with degeneracy of the K and K' points.

When the SOC is switched on in the calculation, the spin degeneracy of the bands is lifted, resulting in valence and conduction band splittings of 33 meV, see Table I, with a small band gap of 0.7 meV, see the right hand side of Fig. 2(a). A similar behavior has been observed for graphene on Bi<sub>2</sub>Te<sub>3</sub> and MoTe<sub>2</sub><sup>11</sup>. The characteristic shape of the bands near the Fermi

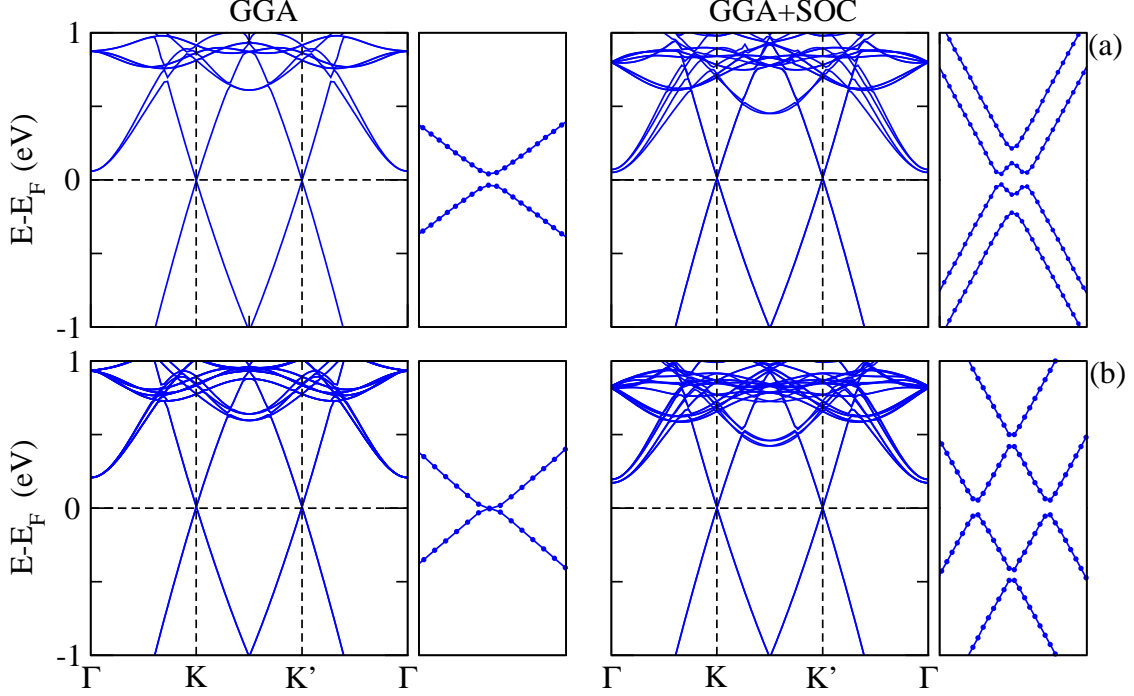


FIG. 2. GGA and GGA+SOC band structures for (a) graphene on  $\text{WS}_2$  and (b) graphene sandwiched between  $\text{WS}_2$  layers. Zoomed views of the K point are shown to clarify the band splitting.

level signifies a QSH phase (band inversion under preserved time-reversal symmetry), similar to the observations in  $\text{InAs}/\text{GaSb}^{22}$ . It should be noted that the bands above and below the Fermi level have opposite spin in agreement with the signature of the QSH phase. A similar picture appears in germanene nanorods embedded in fully H-passivated germanene<sup>23</sup> and in two-dimensional  $\text{Sn}^{24}$ , for which the gap can be strongly enhanced by the application of the strain such that devices can operate at room temperature.

In Fig. 2(b) we present results for graphene sandwiched between  $\text{WS}_2$  layers. We find a 0.1 meV band gap without SOC and one of 1.1 meV when the SOC is taken into account. The shape of the band structure again reflects a QSH state. Larger valence and conduction band splittings of 92 meV and 99 meV, respectively, are achieved because two  $\text{WS}_2$  layers are attached to the graphene, see Table 1, similar to the 70 meV band splitting of graphene in contact with the (111) surface of  $\text{BiFe}_3$  (which is magnetic and thus hosts a quantum anomalous Hall effect<sup>25</sup>).

We also study hybrid systems with monolayer  $\text{WSe}_2$ , which is a semiconductor with a band gap of 1.65 eV<sup>26</sup>. The binding energy of graphene on  $\text{WSe}_2$  turns out to be 54 meV and thus is similar to the  $\text{WS}_2$  case. On the other hand, the band gap of 3.6 meV, see

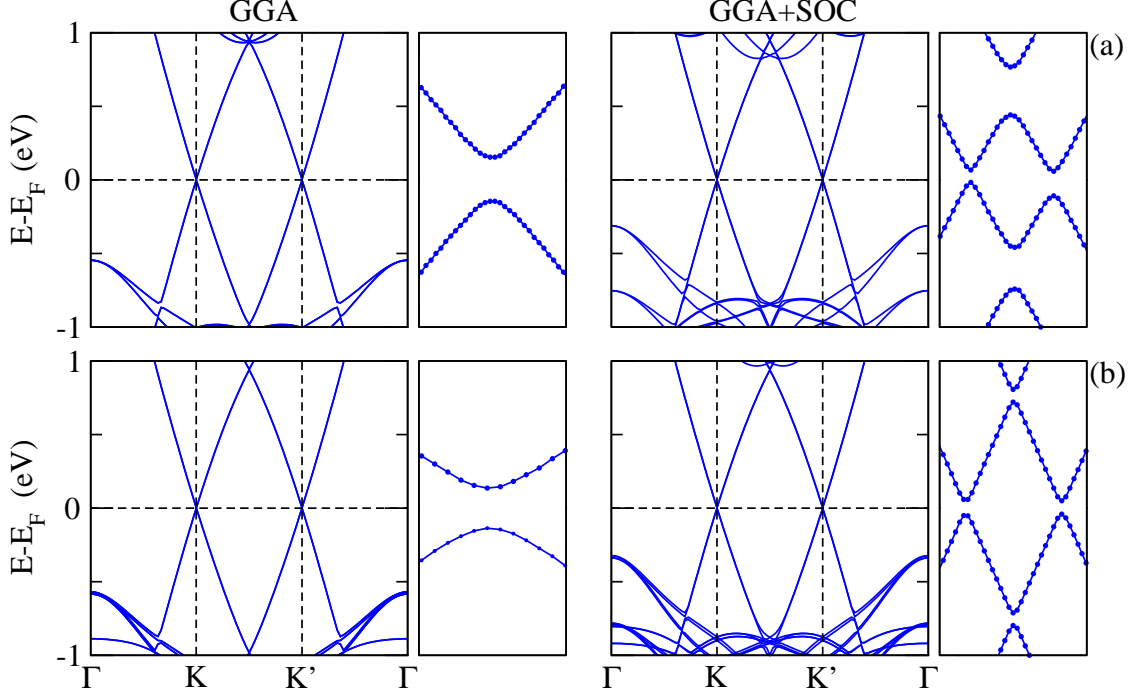


FIG. 3. GGA and GGA+SOC band structures for (a) graphene on WSe<sub>2</sub> and (b) graphene sandwiched between WSe<sub>2</sub> layers. Zoomed views of the K point are shown to clarify the band splitting.

Fig. 3(a), is about 5 times larger than for WS<sub>2</sub>, reflecting the stronger SOC in WSe<sub>2</sub>. A comparison of the bulk properties of WS<sub>2</sub> and WSe<sub>2</sub> can be found in Refs.<sup>27,28</sup>, for example. Again, according to Fig. 3(a), the spin degeneracy at the K and K' points is lifted under inclusion of the SOC. The band structure qualitatively reflects the same characteristics as demonstrated for WS<sub>2</sub> in Fig. 2(a). However, the valence and conduction band splittings are enhanced to 145 meV and 132 meV, respectively, and so is the band gap (0.9 meV), see the zoomed view in Fig. 3(a). This finding is in agreement with the fact that the spin splitting due to SOC is about 50 meV larger in bulk WSe<sub>2</sub> than in bulk WS<sub>2</sub><sup>27,28</sup>. For graphene sandwiched between WSe<sub>2</sub> layers, we find a reduction of the band gap from 3.0 meV to 1.0 meV under SOC with enhanced valence and conduction band splittings of 149 meV and 153 meV, respectively, compare Fig. 3(b) to Fig. 2(b), as to be expected from our previous discussion. In the WSe<sub>2</sub> systems the QSH effect therefore is significantly more pronounced than in the WS<sub>2</sub> systems.

## IV. CONCLUSION

Based on first-principles calculations, we have investigate the structural and electronic properties of hybrid systems consisting of graphene and WS<sub>2</sub> or WSe<sub>2</sub>. Band gaps of few meV are obtained due to the interaction between the component materials. Moreover, band inversion is found at the K/K' points, which indicates QSH states. By the preserved time-reversal symmetry together with the enhancement of the effective SOC in graphene, these systems are able to realize topological phases and therefore QSH states. Usually a strong magnetic field is needed to achieve a QSH state in graphene<sup>12</sup>, while we propose systems in that a QSH state appears without magnetic field, which is a great advantage.

---

\* thaneshwor.kaloni@kaust.edu.sa, +1-2049522900

† udo.schwingenschlogl@kaust.edu.sa, +966-544700080

- <sup>1</sup> K. S. Novoselov, V. I. Fal'ko, L. Colombo, P. R. Gellert, M. G. Schwab, and K. Kim, *Nature* **490**, 192 (2012).
- <sup>2</sup> A. K. Geim, *Nature* **499**, 419 (2013).
- <sup>3</sup> S. Bertolazzi, D. Krasnozhan, and A. Kis, *ACS Nano*, **7**, 3246 (2013).
- <sup>4</sup> T. Georgiou, R. Jalil, B. D. Belle, L. Britnell, R. V. Gorbachev, S. V. Morozov, Y.-J. Kim, A. Gholinia, S. J. Haigh, O. Makarovskiy, L. Eaves, L. A. Ponomarenko, A. K. Geim, K. S. Novoselov, and A. Mishchenko, *Nat. Nanotechnol.* **8**, 100 (2013).
- <sup>5</sup> B. A. Bernevig, T. L. Hughes, and S. C. Zhang, *Science* **314**, 1757 (2006).
- <sup>6</sup> A. Roth, C. Brüne, H. Buhmann, L. W. Molenkamp, J. Mauciejko, X. L. Qi, and S. C. Zhang, *Science* **325**, 294 (2009).
- <sup>7</sup> C. L. Kane and E. J. Mele, *Phys. Rev. Lett.* **95**, 226801 (2005).
- <sup>8</sup> Y. Yao, F. Ye, X. L. Qi, S. C. Zhang, and Z. Fang, *Phys. Rev. B* **75**, 041401 (2007).
- <sup>9</sup> C. Weeks, J. Hu, J. Alicea, M. Franz, and R. Wu, *Phys. Rev. X* **1**, 021001 (2011).
- <sup>10</sup> J. Balakrishnan, G. K. W. Koon, M. Jaiswal, A. H. Castro Neto, and B. Özyilmaz, *Nat. Phys.* **9** 284, (2013).
- <sup>11</sup> L. Kou, F. Hu, B. Yan, T. Wehling, C. Felser, T. Frauenheim, and C. Chen, arXiv:1309.6653v1.

- <sup>12</sup> A. F. Young, J. D. Sanchez-Yamagishi, B. Hunt, S. H. Choi, K. Watanabe, T. Taniguchi, R. C. Ashoori, and P. Jarillo-Herrero, *Nature* **505**, 528 (2014).
- <sup>13</sup> W. Bao, Z. Zhao, H. Zhang, G. Liu, P. Kratz, L. Jing, J. Velasco, D. Smirnov, and C. N. Lau, *Phys. Rev. Lett.* **105**, 246601 (2010).
- <sup>14</sup> P. Giannozzi, S. Baroni, N. Bonini, M. Calandra, R. Car, C. Cavazzoni, D. Ceresoli, G. L. Chiarotti, M. Cococcioni, I. Dabo, A. Dal Corso, S. de Gironcoli, S. Fabris, G. Fratesi, R. Gebauer, U. Gerstmann, C. Gougoussis, A. Kokalj, M. Lazzeri, L. Martin-Samos, N. Marzari, F. Mauri, R. Mazzarello, S. Paolini, A. Pasquarello, L. Paulatto, C. Sbraccia, S. Scandolo, G. Sclauzero, A. P. Seitsonen, A. Smogunov, P. Umari, and R. M. Wentzcovitch, *J. Phys.: Condens. Matter* **21**, 395502 (2009).
- <sup>15</sup> G. Kresse and J. Furthmüller, *Comput. Mater. Sci.* **6**, 15 (1996).
- <sup>16</sup> W. S. Yun, S. W. Han, S. C. Hong, I. G. Kim, and J. D. Lee, *Phys. Rev. B* **85**, 033305 (2012).
- <sup>17</sup> A. Taroni, *Nat. Mater.* **12**, 378 (2013).
- <sup>18</sup> D. Braga, I. G. Lezama, H. Berger, and A. F. Morpurgo, *Nano Lett.* **12**, 5218 (2012).
- <sup>19</sup> W. Ki, X.-Y. Huang, J. Li, D. L. Young, and Y. Zhang, *J. Mater. Res.* **22**, 1390 (2007).
- <sup>20</sup> A. Mattheus, A. Ennaoui, S. Fiechter, S. Tiefenbacher, T. Kiesewetter, K. Diesner, I. Sieber, W. Jaegermann, T. Tsirlina, and R. Tenne, *J. Electrochem. Soc.* **144**, 1013 (1997).
- <sup>21</sup> S.-S. Li and C.-W. Zhang, *J. Appl. Phys.* **114**, 183709 (2013).
- <sup>22</sup> C. Liu, T. L. Hughes, X.-L. Qi, K. Wang, and S.-C. Zhang, *Phys. Rev. Lett.* **100**, 236601 (2008).
- <sup>23</sup> L. Seixas, J. E. Padilha, and A. Fazzio, *Phys. Rev. B* **89**, 195403 (2014).
- <sup>24</sup> Y. Xu, B. Yan, H.-J. Zhang, J. Wang, G. Xu, P. Tang, W. Duan, and S.-C. Zhang, *Phys. Rev. Lett.* **111**, 136804 (2013).
- <sup>25</sup> Z. Qiao, W. Ren, H. Chen, L. Bellaiche, Z. Zhang, A. H. MacDonald, and Q. Niu, *Phys. Rev. Lett.* **112**, 116404 (2014).
- <sup>26</sup> C.-H. Chang, X. Fan, S.-H. Lin, and J.-L. Kuo, *Phys. Rev. B* **88**, 195420 (2013).
- <sup>27</sup> A. Ramasubramaniam, *Phys. Rev. B* **86**, 115409 (2012).
- <sup>28</sup> B. Amin, T. P. Kaloni, and U. Schwingenschlögl, *RSC Adv.* **4**, 34561 (2014).